

Antipoisoning Performance of Platinum Catalysts with Varying Carbon Nanotube Properties: Electrochemically Revealing the Importance of Defects

Jianshe Wang,^{*[a, b]} Changhai Liu,^[b, c] Biwei Xiao,^[b] Niancai Cheng,^[b] Adam Riese,^[b] Mohammad Norouzi Banis,^[b] and Xueliang Sun^{*[b]}

To understand the role of functional groups (FGs) and defects in improving the antipoisoning performance of platinum catalysts for formate oxidation, four kinds of supports originating from carbon nanotubes (CNTs) with varying amounts of FGs and varying degrees of defects are discussed. Platinum particles with controlled similarity are deposited onto the four supports to precisely compare the differences between the four supports. The catalysts structures are characterized by XRD, high-resolution TEM, Raman spectroscopy, and XPS. The electrochemical performances of the four catalysts are character-

ized by cyclic voltammetry and chronoamperometry methods. The results show that the use of fully unzipped CNTs, with a higher degree of defects and lower amount of FGs, as a support results in the greatest improvement in antipoisoning performance of platinum, relative to oxidized CNTs with a higher amount of FGs and lower degree of defects. These results indicate that CNT defects play a greater role in promoting the antipoisoning performance of supported catalysts than FGs. These results are helpful to guide the design of supports to improve the antipoisoning performance of formate oxidation catalysts.

1. Introduction

Direct formate fuel cells (DFFCs),^[1–6] featuring several outstanding advantages, have emerged as a new kind of power technology in recent years. Specifically, the overpotential for formate oxidation is lower than that for methanol or ethanol oxidation,^[5] cheap non-platinum materials can be used for the cathode catalysis reaction.^[7–9] Interestingly, formate fuel can be produced from CO₂ electroreduction, which means that DFFCs can run on renewable fuel sources.^[10,11] At present, the anode catalysts for formate oxidation are mainly platinum or palladium based. These families of catalysts suffer from poisoning,^[3,5] which can deteriorate the DFFC performance and also require increased usage of platinum or palladium. Therefore, it is of great significance to improve the antipoisoning performance of anode catalysts for the commercialization of DFFCs.


Poisoning of the anode catalysts is a difficult, common problem encountered with direct liquid fuel cells. One widely accepted reason for this problem is the strong adsorption of CO-like poisoning species on the surface of catalysts.^[12–15] To date, many approaches have been proposed to address this issue, such as introducing transition metals or their oxides,^[16–18] engineering the surface composition of catalysts,^[19,20] and controlling the particle sizes and crystalline facets.^[21,22] In addition to these strategies, it has been demonstrated that the properties of carbon supports, including functional groups (FGs),^[23,24] defects,^[25,26] and graphitic crystallinity,^[27] could modify the antipoisoning performances. Carbon black, carbon nanotubes (CNTs) and graphene nanosheets (GNs), which are three most widely used carbon-based nanomaterials, have been compared as catalyst supports; GNs are proven to be superior.^[28–30] Recently, Xing et al. reported that the Pt activity for methanol and CO oxidation could be enhanced by increasing the degree of oxidation of CNT supports,^[31] this verified the promising potential of modifying the performance of catalysts through facile engineering of the support properties.

However, it is not fully understood what property of carbon supports play the most important role in improving the antipoisoning performance of platinum- or palladium-based catalysts mainly because 1) there are typically several different properties on a given support and 2) there is a lack of established methods to distinguish between subtle differences in the influence of different properties. For example, when introducing FGs by oxidizing CNTs, defects could be formed at the same time; this makes it difficult to compare the roles of defects and FGs. To address this issue, we prepared CNT-based supports with controlled differences in defects and/or FGs and

[a] Prof. J. Wang
School of Chemical Engineering and Energy
Zhengzhou University
Science Road 100, Zhengzhou 450000 (P.R. China)
E-mail: wangjs07@zzu.edu.cn

[b] Prof. J. Wang, Dr. C. Liu, Dr. B. Xiao, Dr. N. Cheng, A. Riese, M. N. Banis, Prof. X. Sun
Department of Mechanical and Materials Engineering
The University of Western Ontario
ON, N6A 5B9 (Canada)
E-mail: wangjs07@zzu.edu.cn
xsun@eng.uwo.ca

[c] Dr. C. Liu
School of Materials Science & Engineering, Changzhou University
Changzhou 213164 (P.R. China)

 The ORCID identification number(s) for the author(s) of this article can be found under <http://dx.doi.org/10.1002/celec.201600589>.

compared the effect of different properties on the antipoisoning performance of catalysts. It should be emphasized that the platinum particles were kept similar by first preparing platinum in one beaker and then dividing this sample into four parts for deposition on different supports, with the aim of merely analyzing the effects of defects and/or FGs without considering differences in platinum. We found that the defects played a more efficient role in improving the antipoisoning performance. We believe that this conclusion is beneficial for guiding the rational engineering of catalyst supports. Furthermore, the method used herein can be proposed as a paradigm for precisely studying the antipoisoning performances of a series of catalysts.

2. Results and Discussion

2.1. Structural Characterization of Pt/CNTs, Pt/O-CNTs, Pt/p-CNTs, and Pt/f-CNTs

The XRD patterns of Pt/CNTs, Pt/O-CNTs, Pt/p-CNTs, and Pt/f-CNTs are shown in Figure 1, and the XRD patterns of CNTs are also collected for reference. Samples denoted O-CNTs indicate CNTs containing high amounts of oxygen-containing functional groups (OFGs) during partial unzipping of CNTs by oxidation. Those O-CNTs annealed at 900 °C in argon to detach OFGs are denoted as p-CNTs which contain smaller amount of OFGs

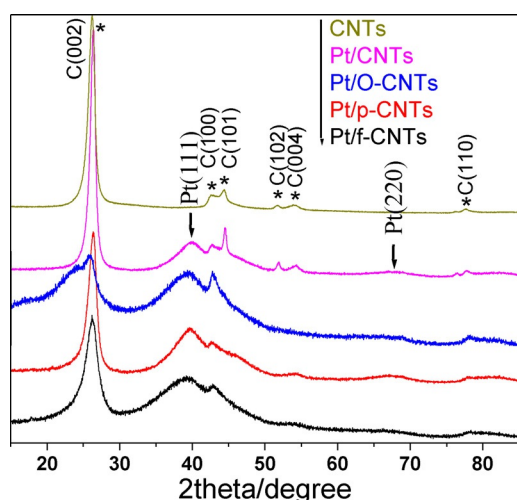


Figure 1. XRD patterns for CNTs, Pt/CNTs, Pt/O-CNTs, Pt/p-CNTs, and Pt/f-CNTs. The asterisks represent the diffraction peaks for the graphitic structure in the CNTs.

than O-CNTs. The f-CNTs indicate those samples of fully unzipped CNTs, which are obtained through a similar process as that for p-CNTs, except that the treatment time is increased to be 10 h.

The peak at 26.4° in the XRD patterns of the five samples can be ascribed to the carbon (002) diffraction. Other peaks at 42.5°, 44.3°, 51.7°, 54.2° and 77.7° can be ascribed to (100), (101), (102), (004) and (110) diffractions of the graphitic framework, respectively.^[32] It is noteworthy that the peak for O-CNTs

is broader than those of the other samples, which indicates that the graphitic integrity is partly destroyed by the severe oxidation treatment. After annealing the O-CNTs at 900 °C in argon to obtain p-CNTs, the graphitic integrity was restored, possibly due to the elimination of FGs,^[33] as seen from the C(002) peak for p-CNTs. The peak at 39.8° for Pt(111) diffraction confirmed the presence of metallic Pt in Pt/CNTs, Pt/O-CNTs, Pt/p-CNTs, and Pt/f-CNTs. As emphasized above, we expect the platinum sizes to be as similar as possible to eliminate size effects. Indeed, we tried to control this by preparing platinum in a single beaker. However, the width of the peak for Pt (111) varies somewhat across the samples. This might be due to the inhomogeneous dispersion of platinum on different supports (e.g. agglomeration; see the discussion of the TEM results). Because inaccuracy would be involved if the Scherrer equation were used to calculate the average platinum grain size, we think it is more reliable to evaluate the platinum size distribution based upon high-resolution TEM (HRTEM) results.

Raman spectra were collected to investigate structural differences in the CNT-based supports for Pt/CNTs, Pt/O-CNTs, Pt/p-CNTs, and Pt/f-CNTs (Figure 2). For each sample, there are two

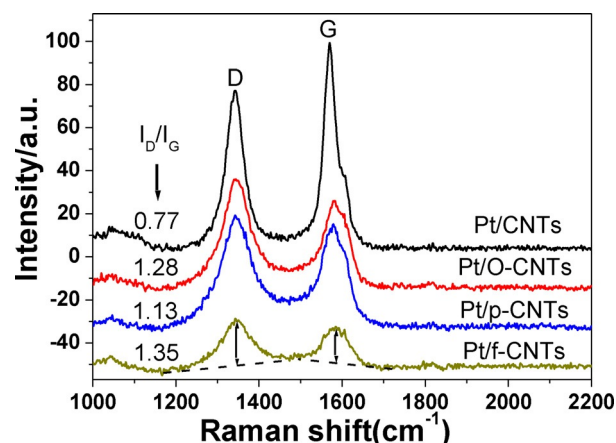


Figure 2. Raman spectra for Pt/CNTs, Pt/O-CNTs, Pt/p-CNTs, and Pt/f-CNTs.

characteristic bands at $\tilde{\nu} \approx 1340 \text{ cm}^{-1}$ and 1580 cm^{-1} that can be ascribed to the D and G bands, respectively.^[34–36] The D band represents the sp^3 -hybridized carbon, namely, disordered carbon, whereas the G band originates from the sp^2 -hybridized carbon, namely, graphitized carbon. The ratio of the D band intensity to the G band intensity, denoted as I_D/I_G , can be used to characterize the degree of defects within a carbon material.^[34–36] The estimated values of I_D/I_G for each sample are listed in Figure 2. These values clearly show that f-CNTs possess the highest I_D/I_G value, which indicates that f-CNTs possess the highest degree of defects.

Notably, the amount of FGs and degree of defects were designed to vary for the CNTs, O-CNTs, p-CNTs, and f-CNTs, as illustrated in Figure 3. As confirmed by the Raman spectroscopy results, the degree of defects for CNTs, p-CNTs, and f-CNTs indeed increased due to the increasing oxidation intensity during sample treatment. For O-CNTs and p-CNTs, we expected

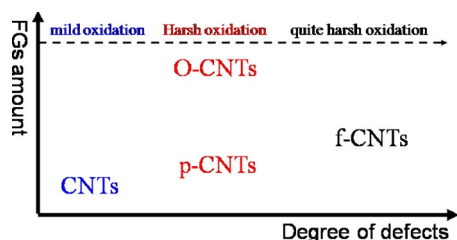


Figure 3. The expected trend in the amount of FGs and degree of defects for the CNT-based supports.

more FGs formed on O-CNTs with similar degrees of defects on the two supports. It is easy to find evidence of the higher amount of FGs on O-CNTs from XPS results. However, it seems to be difficult to assume a similar degree of defects from the higher $I_{\text{O}}/I_{\text{C}}$ value for O-CNTs than that for p-CNTs. Even if the degree of defects of O-CNTs was really higher than that of p-CNTs, our final conclusion that defects play a more important role in improving anti-poisoning performance than FGs would not be influenced (see below).

To examine the FGs in detail for the four as-prepared catalysts, XPS spectra were recorded and deconvoluted to determine the C 1s information (Figure 4). The amount of FGs can be quantitatively compared from the proportion of C–O and C=O on the four supports, as shown in Table 1. It can be seen

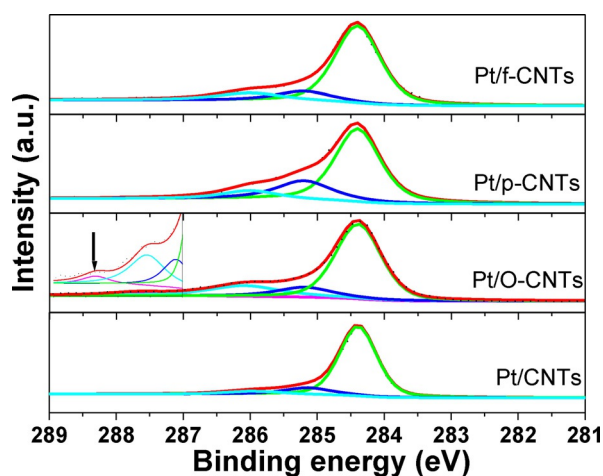


Figure 4. XPS results for the C 1s spectra. The inset shows an enlargement of part of the XPS profile for Pt/O-CNTs.

Table 1. Detailed analysis of the C 1s spectra shown in Figure 4.					
		Pt/CNTs	Pt/O-CNTs	Pt/p-CNTs	Pt/f-CNTs
C–C (sp^2)	position [eV]	284.4	284.4	284.4	284.4
	proportion [%]	78.7	64.8	65.4	73.4
C–C (sp^3)	position [eV]	285.2	285.3	285.2	285.2
	proportion [%]	12.8	13.2	24.0	13.9
C–O	position [eV]	286.1	286.2	286.1	286.1
	proportion [%]	5.5	18.4	10.6	12.7
C=O	position [eV]	–	287.8	–	–
	proportion [%]	–	3.6	–	–

that O-CNTs feature the highest total proportion of C–O and C=O; this indicates a far higher amount of FGs for O-CNTs in comparison with CNTs, p-CNTs, and f-CNTs. Comparing the amount of FGs in the CNTs with those of p-CNTs and f-CNTs, it can be seen that a clear increase in the amount of FGs were observed for p-CNTs and f-CNTs, although these two samples were annealed at 900 °C to detach OFGs. This result reflects the higher unzipped nature of p-CNTs and f-CNTs. With unzipping treatment, more nonbonded carbon atoms would form at the graphene-like edges, which are prone to being oxidized, resulting in the relatively higher concentration of FGs.

TEM images of Pt/CNTs, Pt/O-CNTs, Pt/p-CNTs, and Pt/f-CNTs are shown in Figure 5 a–d accompanied by the corresponding Pt size distribution histograms. From Figure 5 a, it can be seen that Pt particles are unevenly dispersed on the CNT surfaces with a few agglomerates (see blue circles); this indicates a sparsity of sites for Pt attachment due to the low amounts of FGs and defects. The Pt size distribution histogram for Pt/CNTs obtained by statistically calculating 120 isolated Pt particles from the enlarged HRTEM image indicates that the average Pt size is about 1.6 nm. The Pt size distribution histograms for Pt/O-CNTs, Pt/p-CNTs, and Pt/f-CNTs are similar to that of Pt/CNTs. This is understandable considering that the Pt particles were first prepared and then divided into four parts for deposition onto the four CNT-based supports. Thus, the differences in electrochemical performance can be merely attributed to differences in support properties with no need to consider the platinum size effect.

Comparing Figure 5 b with 5 a, one can see that the dispersion of Pt on O-CNTs is more homogeneous, which indicates more available sites for Pt deposition. Most of the O-CNT surfaces have been etched by oxidation during partial unzipping, as indicated by the red rectangle. Severe oxidation also produced partly exfoliated graphene sheets (see red arrows). The TEM image of Pt/p-CNTs in Figure 5 c is similar to that of Pt/O-CNTs, as seen from the unzipped nanotubes (see red rectangle) and exfoliated graphene sheets (see red arrows).

From Figure 5 d, one can see more graphene nanoribbons (red arrows) in comparison with those in Figure 5 b and c; this indicates the most severe oxidation involved in the preparation of f-CNTs. The Pt particles are homogeneously and densely dispersed on f-CNTs, which indicates a high concentration of adsorption sites for Pt; this is in good agreement with the highest Pt content of this sample [inductively coupled plasma (ICP): 14 wt%].

2.2. Electrocatalytic Performance of Pt/CNTs, Pt/O-CNTs, Pt/p-CNTs, and Pt/f-CNTs

For electrochemical characterization of each Pt catalyst, stable cyclic voltammograms were first recorded in 1 M KOH and 1 M KOH + 1 M HCOOK. Then, after cleaning the catalysts by keeping the electrode potential at 0.2 V for 3 s, two cycles of cyclic voltammetry (CV), ranging from –0.8 to 0.2 V, were recorded in 1 M KOH + 1 M HCOOK at 50 and 10 mVs^{-1} (Figure 6). The corresponding cyclic voltammograms in 1 M KOH were also recorded at 50 mVs^{-1} for reference (black dashed lines).

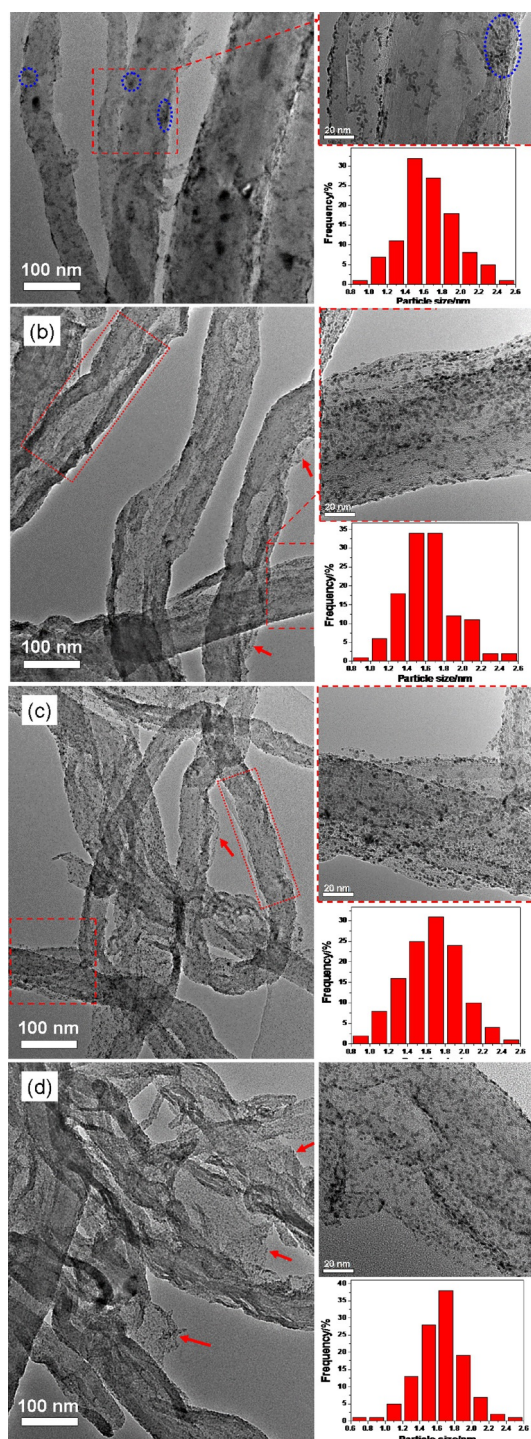


Figure 5. TEM images for a) Pt/CNTs, b) Pt/O-CNTs, c) Pt/p-CNTs, and d) Pt/f-CNTs accompanied by corresponding HRTEM graphs and Pt size distribution histograms.

To best analyze the electrochemical performance of each catalyst, it is necessary to understand the details of CV profiles. Taking Figure 6a as an example, two peaks (peak 1 and peak 2) for each CV curve can be seen during formate oxidation; peak 1 can be ascribed to the direct oxidation of formate, whereas peak 2 indicates the oxidation of poisoning species.^[3,4] Bearing this in mind, we can analyze the antipoisoning per-

formance of a catalyst by comparing the variation of peaks 1 and 2 in the first and second cycles. As seen from the second cycle (Figure 6, blue curve), the current of peak 1 decreases somewhat, whereas that of peak 2 increases, which indicates the formation of poisoning species during the lower potential portion of the scan. The formation of poisoning species can also be verified from the diminished H desorption profiles for the cyclic voltammograms of the second cycle in comparison with the first cycle. To observe more clearly the effect of poisoning species on catalyst performance, cyclic voltammograms were recorded at a lower scanning rate (Figure 6e–h). At a lower scanning rate, there is more time for poisoning species to accumulate on platinum surfaces, which should cause a greater decrease in peak 1 in the second cycle. Therefore, the extent of the decrease of peak 1 (denoted as I_1/I_2 , in which I_1 and I_2 represent the currents of peak 1 for the first and second cycles, respectively) can be used to evaluate the antipoisoning performance of each catalyst (Table 2).

Table 2. Antipoisoning performances of Pt/CNTs, Pt/O-CNTs, Pt/p-CNTs, and Pt/f-CNTs, as determined by analysis of the CV results.

Catalyst (scan rate [mV s^{-1}])	I_1 [$\text{mA mg}_{\text{Pt}}^{-1}$]	I_2 [$\text{mA mg}_{\text{Pt}}^{-1}$]	I_1/I_2
Pt/CNTs (50)	258	240	1.08
Pt/O-CNTs (50)	260	256	1.01
Pt/p-CNTs (50)	266	252	1.06
Pt/f-CNTs (50)	237	237	1.00
Pt/CNTs (10)	221	144	1.53
Pt/O-CNTs (10)	190	146	1.30
Pt/p-CNTs (10)	198	151	1.31
Pt/f-CNTs (10)	188	150	1.25

In Table 2, the ratio of I_1 to I_2 (I_1/I_2) means the decreasing extent of the current of peak 1 due to poisoning species formed in the second cycles. A higher value of I_1/I_2 represents a higher tendency of poisoning. From the results in Table 2, we can see that the values of I_1/I_2 for the four catalysts at 50 mV s^{-1} are slightly different. When lowering the scanning rate to 10 mV s^{-1} , the values of I_1/I_2 for the four catalysts all increased due to the increased accumulation of poisoning species and the differences between these values became more discernible. Specifically, the I_1/I_2 values for the four catalysts follow an increasing trend of Pt/f-CNTs < Pt/O-CNTs \approx Pt/p-CNTs < Pt/CNTs, which indicates that Pt/f-CNTs exhibit the best antipoisoning performance.

To further compare the antipoisoning performance of the four catalysts, their quasi-steady currents of formate oxidation were recorded at -0.5 V for 2000 s (Figure 7). The initial currents for the four catalysts all dropped sharply in the earlier time range and then corresponding quasi-steady currents were achieved. The final currents at 2000 s follow a decreasing trend of Pt/f-CNTs > Pt/O-CNTs > Pt/p-CNTs > Pt/CNTs, which again indicates that Pt/f-CNTs are superior to the other three catalysts in terms of antipoisoning performance.

Because the initial CV currents at -0.5 V are different for the four catalysts (see Figure 6), it is reasonable to use the CV cur-

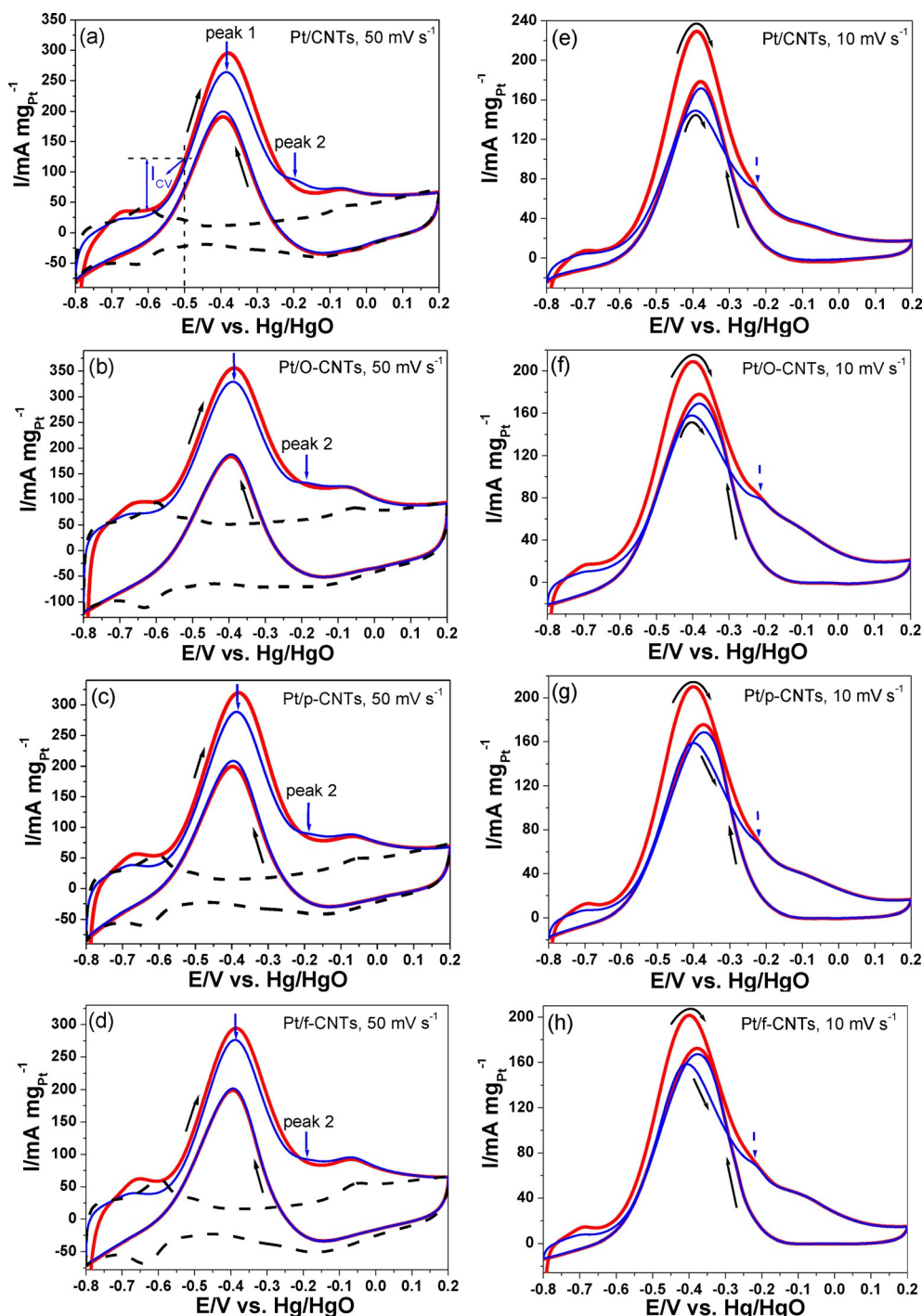


Figure 6. Cyclic voltammograms recorded in 1 M KOH + 1 M HCOOK for a) Pt/CNTs, b) Pt/O-CNTs, c) Pt/p-CNTs, and d) Pt/f-CNTs at 50 mV s⁻¹ and e) Pt/CNTs, f) Pt/O-CNTs, g) Pt/p-CNTs, and h) Pt/f-CNTs at 10 mV s⁻¹. The red and blue lines represent the first and second cycles, respectively. The black dashed lines in a)–d) represent the cyclic voltammograms recorded in 1 M KOH at 50 mV s⁻¹.

rents (I_{CV}) as a reference to evaluate the decaying extent of CA currents (I_{CA}). To some extent, I_{CV} represents the activity of a catalyst with negligible (or slight) suppression by poisoning species, since it is obtained at fast scanning rates (usually 50 mV s⁻¹), whereas I_{CA} represents the activity suppressed by poisoning species. The ratio of I_{CA} to I_{CV} (I_{CA}/I_{CV}) can reflect the extent of poisoning or antipoisoning performance of a catalyst. Thus, we further calculated the value of I_{CA}/I_{CV} for each catalyst,

Table 3. Analysis of antipoisoning performances by using the values of I_{CA} and I_{CV}			
	I_{CA} [mA mg _{Pt} ⁻¹]	I_{CV} [mA mg _{Pt} ⁻¹]	I_{CA}/I_{CV} [%]
Pt/CNTs	10.4	81.2	12.8
Pt/O-CNTs	18.7	94.4	19.8
Pt/p-CNTs	17.4	92.3	18.9
Pt/f-CNTs	20.0	80.9	24.7

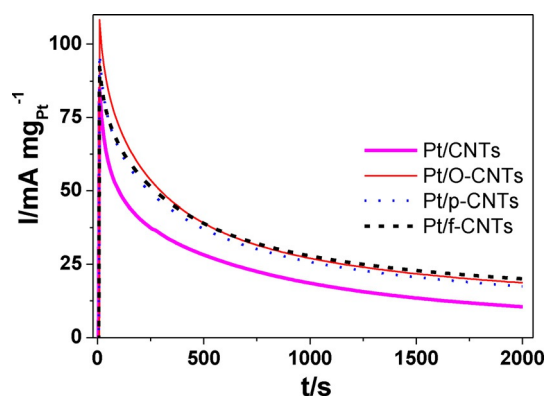


Figure 7. Chronoamperometry (CA) curves recorded at -0.5 V in 1 M KOH + 1 M HCOOK for Pt/CNTs, Pt/O-CNTs, Pt/p-CNTs, and Pt/f-CNTs.

in which I_{CA} refers to the CA final current and I_{CV} refers to the corresponding CV current (at -0.5 V) obtained from the forward scanning curve, as exemplified in Figure 6a. The calculated results are listed in Table 3. From the results shown in Table 3, we can see that the values of I_{CA}/I_{CV} follow a decreasing trend of Pt/f-CNTs > Pt/O-CNTs \approx Pt/p-CNTs > Pt/CNTs; this further indicates the superior antipoisoning performance of Pt/f-CNTs. It should be noted that the I_{CA}/I_{CV} value of Pt/f-CNTs is nearly 25% higher than those of Pt/O-CNTs or Pt/p-CNTs, whereas the I_{CA}/I_{CV} values of Pt/O-CNTs and Pt/p-CNTs are similar. By only comparing the values of I_{CA} (Table 3), the difference between Pt/f-CNTs, Pt/O-CNTs, and Pt/p-CNTs is not so distinct; this indicates the necessity of using I_{CV} as a reference when evaluating the I_{CA} .

From the above results, we know that Pt/f-CNTs exhibit the best antipoisoning performance among the four catalysts. Because O-CNTs have more FGs and less defects than those of f-CNTs, while Pt/O-CNTs is inferior to Pt/f-CNTs in terms of antipoisoning performance, we can conclude that the role played by the FGs is negligible in comparison with that by defects. This can be further supported by comparing Pt/O-CNTs with Pt/p-CNTs. As seen from the values of I_1/I_2 in Table 2 and I_{CA}/I_{CV} in Table 3, the antipoisoning performance of Pt/O-CNTs is only slightly higher than that of Pt/p-CNTs. Considering the greater amount of FGs in O-CNTs than those in p-CNTs (see the XPS results), this slight difference in antipoisoning performance suggests that FGs play a minor role in improving poisoning tolerance, when compared with defects, although FGs might indeed have a small positive effect. As analyzed from the higher I_D/I_G value of O-CNTs than that of p-CNTs, it is possible that O-CNTs has a higher degree of defects than those in p-CNTs. Thus, the role played by FGs can be further neglected when compared with the role of defects because the antipoisoning performance of Pt/O-CNTs is only negligibly higher than that of Pt/p-CNTs.

To further probe the difference between the four catalysts, CO stripping was conducted (Figure 8). Pt/O-CNTs, Pt/p-CNTs, and Pt/f-CNTs, in comparison with Pt/CNTs, all exhibited superior activity, as determined by the lower onset potentials (about -0.63 versus -0.58 V) and peak 1 potentials (see black dashed line in Figure 8). This can again be attributed to their higher

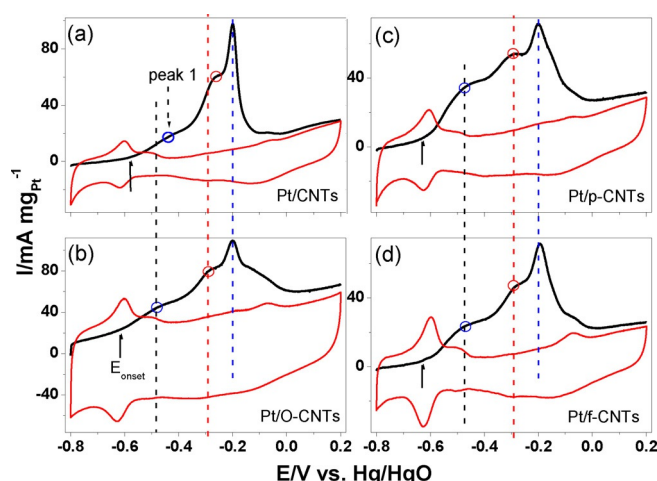


Figure 8. Curves for CO stripping on a) Pt/CNTs, b) Pt/O-CNTs, c) Pt/p-CNTs, and d) Pt/f-CNTs recorded at 20 mV s^{-1} in 1 M KOH.

concentration of FGs and defects than those in CNTs, and indicates the positive effects of FGs and defects on improving the antipoisoning performance. Because the role of FGs is small relative to the effects of defects (see the above analysis from CV and CA results), the superior CO oxidation performances of Pt/O-CNTs, Pt/p-CNTs, and Pt/f-CNTs to that of Pt/CNTs can be explained with respect to the higher degree of defects in the three supports. However, as seen from Figure 8c and d, the profiles of CO stripping on Pt/O-CNTs, Pt/p-CNTs, and Pt/f-CNTs are similar, which indicates that the differences between the three catalysts cannot be distinguished by the CO stripping method. This further justified the necessity of using I_1/I_2 and I_{CA}/I_{CV} as an index when evaluating the antipoisoning performance of catalysts.

To investigate the reason for the superior antipoisoning performance of Pt/f-CNTs, XPS spectra of the Pt4f peak were collected and deconvoluted into two pairs of doublets (Figure 9), which were calibrated by setting the C1s peak of CNTs at 284.4 eV. The more intense doublet (blue curves) could be ascribed to platinum(0), whereas the weaker doublet (magenta curves) with higher binding energies (BEs) could be assigned

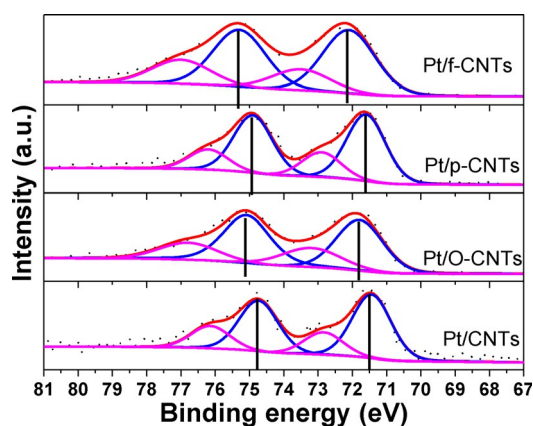


Figure 9. XPS spectra of the Pt4f region of Pt/CNTs, Pt/O-CNTs, Pt/p-CNTs, and Pt/f-CNTs.

to platinum in an oxidized state. The BEs of platinum for the four catalysts follow an increasing trend of Pt/f-CNTs > Pt/O-CNTs > Pt/p-CNTs > Pt/CNTs; this is in good agreement with the trend observed in Tables 2 and 3. This result indicates that the interaction between Pt and f-CNTs is the strongest among the four samples due to the highest degree of defects for f-CNTs. With this interaction and corresponding electron transfer from Pt to f-CNTs, fewer electrons could be shared by CO species adsorbed on the Pt surface,^[37–39] leading to weaker binding of CO on Pt and the superior antipoisoning performance of Pt/f-CNTs. It is also evident that the BE of Pt for Pt/O-CNTs is higher than that of Pt/p-CNTs, but the antipoisoning performance of the former is only slightly higher than that of the latter. The reason for this result is beyond our understanding at present.

Finally, we want to emphasize that this research is meaningful in providing a set of detailed methods for analyzing subtle differences between several catalysts. Electrochemical methods (by using I_1/I_2 and I_{CA}/I_{CV}), combined with Raman and XPS spectra, consistently and undoubtedly corroborate our judgment that defects have a more positive effect than that of FGs. Certainly, we also admit that our insight into the effect of FGs on antipoisoning performance is preliminary and further study on the effects of FG types and amounts is necessary.

3. Conclusions

The antipoisoning performance of CNT-supported platinum catalysts were improved by increasing the extent of CNT unzipping; this could be explained by stronger electronic interactions between platinum and supports, possibly caused by increasing defects on the carbon structure. Compared with defects, the FGs introduced by oxidizing the CNT surfaces had limited effect on improving the antipoisoning performance of platinum catalysts. These results demonstrated the potential for controlling the support properties and corresponding interaction between catalysts and supports for the purpose of enhancing the antipoisoning performance of formate oxidation catalysts.

Experimental Section

Chemicals

Multiwalled CNTs, with an average diameter of 40–60 nm, were provided by Shenzhen Nanotech Port Co., Ltd. Other reagents of analytical purity were used without further purification.

Preparation of CNT-Based Supports

Pristine CNTs were first ultrasonicated in a 20 wt% solution of HNO₃ for 30 min to introduce OFGs for Pt nanoparticle attachment. After filtration, aqueous washing, and drying, the treated CNTs were collected for use.

Partial unzipping of CNTs was achieved by following a modified Hummers method.^[40,41] CNTs (100 mg) were dispersed in H₂SO₄ (3.4 mL; 98%, Aldrich) through strong agitation. The viscous solution was then placed in an ice bath before NaNO₃ (75 mg; 99.9%, Aldrich) was added. In the next step, KMnO₄ (450 mg; 99.9%, Al-

drich) was slowly added to the mixture under stirring. After reacting for a certain time, H₂O₂ (2 mL; 30%, Aldrich) was added to the slurry to remove residual KMnO₄. The mixture was subsequently washed with water five times and dried. Because high amounts of OFGs were introduced, the obtained samples were denoted as O-CNTs. To detach the OFGs for subsequent comparison, O-CNTs were annealed at 900 °C in Ar and the obtained samples were denoted as p-CNTs, which contained less OFGs than the O-CNT sample. The fully unzipped CNTs were obtained through a similar process, except the treatment time was increased to 10 h. After annealing at 900 °C in Ar, the samples were collected and denoted as f-CNTs.

Preparation of Pt Catalysts Supported on CNT-Based Supports

Pt precursor was reduced by ethylene glycol (EG) through the microwave-assisted polyol method.^[42] Briefly, EG (100 mL) in a beaker containing H₂PtCl₆·6H₂O (56 mg) and NaOH (200 mg) was heated to boiling with microwave irradiation. The obtained Pt nanoparticles in EG were simultaneously added dropwise into four beakers, each containing CNT-based supports (30 mg; CNTs, O-CNTs, p-CNTs, and f-CNTs). After Pt deposition under magnetic stirring for 3 h, all samples were filtered, washed, and dried in a vacuum oven at 70 °C. The samples were denoted as Pt/CNTs, Pt/O-CNTs, Pt/p-CNTs and Pt/f-CNTs, respectively. The Pt contents of each catalyst were determined, by using an ICP emission spectrometer, to be 5, 11, 10, and 14 wt%, respectively.

Physical Characterization of Pt/CNTs, Pt/O-CNTs, Pt/p-CNTs, and Pt/f-CNTs

The XRD patterns of CNTs, Pt/CNTs, Pt/O-CNTs, Pt/p-CNTs, and Pt/f-CNTs were recorded on a Bruker D8 Advance X-ray diffractometer with Cu K α as the radiation source. All peaks were calibrated by setting the C 1s peak of CNTs at 284.4 eV.

The morphologies of the catalysts were observed by using a transmission electron microscope (FEI Quanta FRG 200F) operating at 200 kV.

XPS results of the catalysts were recorded on an X-ray photoelectron spectrometer (Kratos Axis Ultra DLD, monochromatic Al K α) in ultrahigh vacuum to examine the electronic structures.

The Raman spectra were recorded with a DXR Raman spectrometer (Thermo Fisher Scientific; excitation laser λ = 532 nm, laser power 2 mW, and aperture 50 μ m pinhole).

Electrochemical Characterization of Pt/CNTs, Pt/O-CNTs, Pt/p-CNTs, and Pt/f-CNTs

Catalyst inks were prepared and coated on a glassy carbon (GC; Φ = 5 mm) electrode. Typically, catalyst (2 mg) was homogeneously mixed with ethanol (600 μ L) containing Nafion[®] (0.4 mg) by ultrasonication for 30 min, then thus-prepared ink (15 μ L) was pipetted onto a GC electrode and dried by using an IR lamp. The theoretical mass loading on the GC electrode was 0.05 mg for each catalyst.

A three-electrode cell was coupled to an Autolab potentiostat/galvanostat (Model PGSTAT-30, Ecochemie, Brinkman Instrument). A GC electrode, a Pt wire electrode, and an Hg/HgO electrode were employed as the working, counter, and reference electrodes, respectively. All potentials were referenced to a Hg/HgO electrode

herein, and all electrochemical experiments were conducted at 25 °C with N₂ protection.

For each catalyst characterization, CV was first conducted at 50 mVs⁻¹ in 1 M KOH to record stable cyclic voltammograms. Then cyclic voltammograms for formate oxidation were recorded in a solution containing 1 M KOH and 1 M HCOOK, followed by recording the corresponding CA curve at -0.5 V for 2000 s. Notably, all working electrodes were first preconditioned at 0.2 V for 3 s to clean the Pt surface, then CV or CA data for formate oxidation were recorded.

For CO stripping tests, CO gas was bubbled into a solution containing 1 M KOH for 30 min, while maintaining a constant potential of -0.8 V during CO adsorption onto the electrocatalysts. Excess CO in solution was purged by bubbling N₂ gas for 20 min. Then two successive cyclic voltammograms were recorded at a scan rate of 20 mVs⁻¹.

Acknowledgements

This research is financially supported by the National Natural Science Foundation of China (U1304215) and the China Scholarship Council (201308410311). This research was also supported by the Natural Sciences and Engineering Research Council of Canada (NSERC), the Canada Research Chair (CRC) Program, Canada Foundation for Innovation (CFI), and the University of Western Ontario.

Keywords: carbon nanotubes · defects · oxidation · platinum · structure–activity relationships

- [1] J. H. Jiang, A. Wieckowski, *Electrochem. Commun.* **2012**, *18*, 41–43.
- [2] A. M. Bartrom, J. Ta, T. Q. Nguyen, J. Her, A. Donovan, J. L. Haan, *J. Power Sources* **2013**, *229*, 234–238.
- [3] J. H. Jiang, J. Scott, A. Wieckowski, *Electrochim. Acta* **2013**, *104*, 124–133.
- [4] J. John, H. S. Wang, E. D. Rus, H. D. Abruna, *J. Phys. Chem. C* **2012**, *116*, 5810–5820.
- [5] J. Noborikawa, J. Lau, J. Ta, S. Z. Hu, L. Scudiero, S. Derakhshan, S. Ha, J. L. Haan, *Electrochim. Acta* **2014**, *137*, 654–660.
- [6] L. Zeng, Z. K. Tang, T. S. Zhao, *Appl. Energy* **2014**, *115*, 405–410.
- [7] H. Y. Zhu, S. Zhang, Y. X. Huang, L. H. Wu, S. H. Sun, *Nano Lett.* **2013**, *13*, 2947–2951.
- [8] D. A. Slanac, W. G. Hardin, K. P. Johnston, K. J. Stevenson, *J. Am. Chem. Soc.* **2012**, *134*, 9812–9819.
- [9] D. S. Geng, Y. Chen, Y. G. Chen, Y. L. Li, R. Y. Li, X. L. Sun, S. Y. Ye, S. Knights, *Energy Environ. Sci.* **2011**, *4*, 760–764.
- [10] S. Zhang, P. Kang, T. J. Meyer, *J. Am. Chem. Soc.* **2014**, *136*, 1734–1737.
- [11] S. Zhang, P. Kang, S. Ubnoske, M. K. Brennaman, N. Song, R. L. House, J. T. Glass, T. J. Meyer, *J. Am. Chem. Soc.* **2014**, *136*, 7845–7848.
- [12] T. Yajima, H. Uchida, M. Watanabe, *J. Phys. Chem. B* **2004**, *108*, 2654–2659.
- [13] Q. Tao, Y. L. Zheng, D. C. Jiang, Y. X. Chen, Z. Jusys, R. J. Behm, *J. Phys. Chem. C* **2014**, *118*, 6799–6808.
- [14] B. Peng, H. F. Wang, Z. P. Liu, W. B. Cai, *J. Phys. Chem. C* **2010**, *114*, 3102–3107.
- [15] Y. T. Kim, M. A. Matin, Y. U. Kwon, *Carbon* **2014**, *66*, 691–698.
- [16] F. Xu, R. Xu, S. C. Mu, *Electrochim. Acta* **2013**, *112*, 304–309.
- [17] F. Li, H. Y. Gong, Y. Wang, H. Zhang, Y. Z. Wang, S. N. Liu, S. Wang, C. W. Sun, *J. Mater. Chem. A* **2014**, *2*, 20154–20163.
- [18] H. X. Liu, N. Tian, M. P. Brandon, Z. Y. Zhou, J. L. Lin, C. Hardacre, W. F. Lin, S. G. Sun, *ACS Catal.* **2012**, *2*, 708–715.
- [19] W. Chen, J. Kim, S. H. Sun, S. W. Chen, *Langmuir* **2007**, *23*, 11303–11310.
- [20] H. X. Zhang, C. Wang, J. Y. Wang, J. J. Zhai, W. B. Cai, *J. Phys. Chem. C* **2010**, *114*, 6446–6451.
- [21] A. Mondal, N. R. Jana, *RSC Adv.* **2015**, *5*, 85196–85201.
- [22] N. F. Yu, N. Tian, Z. Y. Zhou, L. Huang, J. Xiao, Y. H. Wen, S. G. Sun, *Angew. Chem. Int. Ed.* **2014**, *53*, 5097–5101; *Angew. Chem.* **2014**, *126*, 5197–5201.
- [23] Y. Cheng, S. P. Jiang, *Electrochim. Acta* **2013**, *99*, 124–132.
- [24] P. Hernández-Fernández, S. Baranton, S. Rojas, P. Ocón, J. M. Léger, J. L. G. Fierro, *Langmuir* **2011**, *27*, 9621–9629.
- [25] G. Kim, S. H. Jhi, *ACS Nano* **2011**, *5*, 805–810.
- [26] Y. R. Sun, C. Y. Du, M. C. An, L. Du, Q. Tan, C. T. Liu, Y. Z. Gao, G. P. Yin, *J. Power Sources* **2015**, *300*, 245–253.
- [27] J. W. Ma, A. Habrioux, C. Morais, A. Lewera, W. Vogel, Y. Verde-Gomez, G. Ramos-Sanchez, P. B. Balbuena, N. Alonso-Vante, *ACS Catal.* **2013**, *3*, 1940–1950.
- [28] L. Li, G. Wu, B. Q. Xu, *Carbon* **2006**, *44*, 2973–2983.
- [29] R. Escudero-Cid, A. S. Varela, P. Hernandez-Fernandez, E. Fatas, P. Ocon, *Int. J. Hydrogen Energy* **2014**, *39*, 5063–5073.
- [30] J. S. Wang, C. H. Liu, M. N. Banis, N. C. Cheng, A. Riese, S. D. Wang, X. L. Sun, *Int. J. Hydrogen Energy* **2016**, *41*, 936–943.
- [31] M. L. Xiao, J. B. Zhu, J. J. Ge, C. P. Liu, W. Xing, *J. Power Sources* **2015**, *281*, 34–43.
- [32] Y. Q. Zhu, H. G. Zhang, J. H. Zhang, J. Liang, Z. D. Gao, B. Q. Wei, D. H. Wu, *J. Mater. Sci. Lett.* **1994**, *13*, 1104–1105.
- [33] S. F. Pei, J. P. Zhao, J. H. Du, W. C. Ren, H. M. Cheng, *Carbon* **2010**, *48*, 4466–4474.
- [34] L. Xin, F. Yang, S. Rasouli, Y. Qiu, Z. F. Li, A. Uzunoglu, C. J. Sun, Y. Z. Liu, P. Ferreira, W. Z. Li, Y. Ren, L. A. Stanciu, J. Xie, *ACS Catal.* **2016**, *6*, 2642–2653.
- [35] W. Qian, R. Hao, J. Zhou, M. Eastman, B. A. Manhat, Q. Sun, A. M. Go-forth, J. Jiao, *Carbon* **2013**, *52*, 595–604.
- [36] E. D. Grayfer, L. S. Kibis, A. I. Stadnichenko, O. Y. Vilkov, A. I. Boronin, E. M. Slavinskaya, O. A. Stonkus, V. E. Fedorov, *Carbon* **2015**, *89*, 290–299.
- [37] J. B. Zhu, M. L. Xiao, X. Zhao, K. Li, C. P. Liu, W. Xing, *Chem. Commun.* **2014**, *50*, 12201–12203.
- [38] I. Fampiou, A. Ramasubramaniam, *J. Phys. Chem. C* **2013**, *117*, 19927–19933.
- [39] Y. N. Tang, Z. X. Yang, X. Q. Dai, *J. Nanopart. Res.* **2012**, *14*, 844.
- [40] W. S. Hummers, R. E. Offeman, *J. Am. Chem. Soc.* **1958**, *80*, 1339–1339.
- [41] B. W. Xiao, X. F. Li, X. Li, B. Q. Wang, C. Langford, R. Y. Li, X. L. Sun, *J. Phys. Chem. C* **2014**, *118*, 881–890.
- [42] J. S. Wang, X. Guo, C. Y. Song, L. C. Wang, J. H. Zhao, X. P. Qiu, *Acta Phys. Chim. Sin.* **2009**, *25*, 767–772.

Manuscript received: September 26, 2016
Accepted Article published: October 27, 2016
Final Article published: November 10, 2016